Available online at www.sciencedirect.com

ScienceDirect

Geochimica et Cosmochimica Acta 259 (2019) 144–154

Geochimica et Cosmochimica Acta

www.elsevier.com/locate/gca

Potassium isotope systematics of oceanic basalts

Brenna Tuller-Ross [a,*], Bernard Marty [b], Heng Chen [a], Katherine A. Kelley [c], Heather Lee [a], Kun Wang (王昆) [a,*]

[a] Department of Earth and Planetary Sciences and McDonnell Center for the Space Sciences, Washington University in St. Louis, MO 63130, USA

[b] CRPG-CNRS, Université de Lorraine, Vandoeuvre lès Nancy, France

[c] Graduate School of Oceanography, University of Rhode Island, RI 02882, USA

Received 28 November 2018; accepted in revised form 2 June 2019; available online 11 June 2019

Abstract

High-temperature isotope fractionation during partial melting and other igneous differentiation processes has been observed in many non-traditional isotope systems. The potassium (K) isotope system has not been extensively investigated historically due to the lack of high-precision analysis methods; however, the recent development of the Multi-Collector Inductively Coupled Plasma Mass Spectrometer (MC-ICP-MS) now allows for high-precision potassium isotope analysis. In this study, we utilized this new method to analyze 51 geologically, geographically, and geochemically diverse oceanic basalt samples including 32 mid-ocean ridge basalts (MORB), 3 back-arc basin basalts (BABB), and 16 oceanic island basalts (OIB). We observed a limited variation of $^{41}K/^{39}K$ ratios across our spread of samples. This variation in mantle-derived rocks is restricted compared to the large K isotopic fractionation observed in low-temperature systems. The averages of MORBs, BABBs, and OIBs are -0.44 ± 0.17‰ (2sd), -0.44 ± 0.08‰, and -0.41 ± 0.16‰, respectively, and there is no geographical variation (e.g., Indian vs. Pacific MORBs) in terms of K isotopes. Among all samples, there are two outliers, in which we have observed evidence of secondary mineral formation (i.e., palagonite) due to interaction with seawater. These two outliers have a K isotopic composition significantly heavier than other unaltered samples, close to the K isotopic composition of seawater. The grand average of all pristine samples is -0.43 ± 0.17‰ (2sd) which agrees well with the Bulk Silicate Earth (BSE) value previously defined. This new study indicates the homogeneity of K isotopes in the mantle and suggests that, since K will not resolvably fractionate during partial melting, any observable fractionation of K isotopes in primitive basalts is likely due to low-temperature, post-eruptive alteration processes. This conclusion is critical for understanding the initial bulk composition of the Earth and it is essential for any interplanetary comparison.

Keywords: Potassium isotopes; MC-ICP-MS; MORB; OIB; BABB

1. INTRODUCTION

The implications of understanding potassium (K) geochemistry are numerous. K is an incompatible lithophile, fluid-mobile alkali metal, and is the eighth most abundant element in the Earth's crust and the fifteenth most abundant element in the bulk Earth (McDonough and Sun, 1995; Rudnick and Gao, 2003). It has only two stable isotopes, ^{39}K (abundance 93.26%) and ^{41}K (6.73%), and one long-lived radioactive isotope, ^{40}K (abundance 0.01%, $t_{1/2} \sim 1.25$ Gyr), which decays to ^{40}Ar and ^{40}Ca (de Laeter et al., 2003). Due to its incompatibility during melt-

* Corresponding authors.
E-mail addresses: brenna@wustl.edu (B. Tuller-Ross), wangkun@wustl.edu (K. Wang).

https://doi.org/10.1016/j.gca.2019.06.001
0016-7037/

ing and mobility in fluid, K preferentially enters melts/fluids, allowing it to potentially be used as a tracer during subduction, crust-mantle interaction, surface silicate weathering, and seafloor reverse weathering processes (Teng et al., 2017; Santiago Ramos et al., 2018).

The K isotope system was first extensively investigated by Humayun and Clayton in 1995, who found no significant K isotope fractionation among any terrestrial samples. However, in the last two years, this conclusion has been revised due to the improved precision of analytical techniques using Multi-Collector Inductively Coupled Plasma Mass Spectrometry (MC-ICP-MS) (Li et al., 2016; Wang and Jacobsen, 2016; Morgan et al., 2018; Hu et al., 2018). So far, few samples have been analyzed for their K isotope compositions using these new high-precision techniques, and we are still faced with two unknowns: the K isotope composition of the mantle, and whether or not the mantle is homogeneous for K isotopes.

Traditionally, mantle xenoliths have been used to infer the composition of the lithospheric mantle (Pearson et al., 2003). However, the K abundance of mantle xenoliths is extremely low (avg = 0.05% K_2O by weight, McDonough, 1990; Pearson et al., 2003) and the precise analysis of low-K samples is challenging due to issues such as column saturation, blank contamination, and matrix effects in MC-ICP-MS. In contrast, oceanic basalts are partial melts from Earth's mantle. During partial melting, K (as an incompatible element) quantitatively enters the melt. Thus, the K isotope composition of basalts represent those of their sources and can be used to probe the composition of the mantle.

Oceanic basalts are classified first by tectonic setting: mid-ocean ridge basalts (MORBs), back-arc basin basalts (BABBs), and oceanic island basalts (OIBs). These different oceanic basalts have different isotopic and chemical compositions and likely sample different depths and lithologies within Earth's mantle. Thus, studying the K isotopic compositions of MORBs, BABBs, and OIBs allows us to infer their mantle sources and helps us to better understand the chemical and isotopic structure of the Earth.

Previously, Wang and Jacobsen (2016a) found no measurable K isotopic differences among 3 basalt samples from various tectonic settings (one MORB, one OIB, and one continental flood basalt). So far, this conclusion has been supported by other studies on several basaltic geostandards distributed by the United States Geological Survey (USGS) (Li et al., 2016; Morgan et al., 2018; Hu et al., 2018); however, there has not yet been a systematic study of K isotopic compositions of oceanic basalts. In this study, we survey a much wider range of samples from geologically, geographically, and geochemically different locations, namely the Mid-Atlantic Ridge, East Pacific Rise, North Fiji Basin, Red Sea, Gulf of Aden, Polynesian Islands, Galapagos, and Hawaii. The major objectives of this study are to (1) investigate potential K isotope heterogeneity in the mantle, (2) identify the controlling factors of any K isotopic variation (if any) in oceanic basalts, and (3) better define the bulk silicate Earth value for the purpose of interplanetary comparison.

2. MATERIALS

We selected a set of 51 basalt samples comprising 32 MORB glasses, 3 BABBs, and 16 OIBs from a wide range of geographic locations and geochemical character. Major- and trace-element abundances have been reported elsewhere (Fisk et al., 1982; Schilling et al., 1983; Marty and Zimmermann, 1999; le Roux et al., 2002; Kelley et al., 2013; Teng et al., 2013). A complete list of samples and a map giving sample source locations are presented in Table 1 and Fig. 1, respectively.

MORBs can be divided into five main types: D (depleted), N (normal), T (transitional), E (enriched), and P (plume-influenced). Since rare earth element (REE) analyses (e.g., La/Sm) were not available for all samples, MORB type determination in this study was limited to the three classes (N, E, and T) that can be determined using K_2O/TiO_2 (see Table 1 footnotes) according to Marty and Zimmerman (1999). The MORB samples in this study include pristine N-MORB, T-MORB, and E-MORB samples sourced from quenched submarine magmas located at various ridge sections; of our 32 total MORB samples, 14 are from the Mid-Atlantic Ridge, 10 are from the East Pacific Rise, 3 are from the Red Sea, 1 is from the Galapagos Spreading Center, and 4 are from the Gulf of Aden (Fig. 1). Samples vary in chemical composition, with Mg, K, and Ti abundances ranging from 6.7 to 9.2 wt.% MgO, 0.04 to 0.38 wt.% K_2O, and 0.76 to 2.11 wt.% TiO_2 (Fig. 2) with K_2O/TiO_2 ratios ranging from 0.02-0.25.

The 3 BABBs are from the North Fiji Basin and are not resolvably influenced by subduction processes and thus their major and trace element geochemistry are effectively indistinguishable from that of MORBs. Samples vary in Mg, K, and Ti composition from 7.31 to 7.46 wt.% MgO, 0.12 to 0.24 wt.% K_2O, and 1.59 to 1.60 wt.% TiO_2, with K_2O/TiO_2 ratios ranging from 0.07-0.15 (Marty and Zimmermann, 1999; Teng et al., 2013).

Oceanic island basalts (OIBs) are often sourced from the deep mantle (relative to MORBs) and typically are isotopically and chemically more variable than MORBs (Hofmann, 1997). This heterogeneity can be accounted for by the involvement of at least five mantle end members: HIMU (high 'μ', or high $^{238}U/^{204}Pb$), EM-1 and EM-2 (enriched mantle 1 and 2, respectively), FOZO (Focal Zone), and DMM (depleted MORB mantle) (Zindler and Hart, 1986; Hart et al., 1992; Stracke et al., 2005; Jackson and Dasgupta, 2008). The isotopic differences between endmembers likely originate from differences in crustal recycling, different degrees of melt extraction, and potential core-mantle interactions (Garnero et al., 2007; Hofmann, 2007; Tkalčić et al., 2016). The 16 OIB samples investigated in this study are mainly pristine basaltic glasses from Hawaii ($n = 2$), the Cook-Austral chain ($n = 2$), and the Society Plume ($n = 12$), and together with the MORB samples reflect contributions from at least 4 mantle endmembers (see Appendix A).

Table 1
Potassium isotopic compositions of oceanic basalts.

Sample	Type [a]	Location	Amount dissolved (mg)	K_2O%	$\delta^{41}K$	95% c.i[b].	n[c]
BABBs							
ST2 17 10		North Fiji Basin	41.7	0.24	−0.50	0.03	12
ST2 17 6		North Fiji Basin	53.7	0.22	−0.43	0.02	12
ST2 17 7		North Fiji Basin	47.2	0.12	−0.40	0.03	12
MORBs							
CH98 DR08	N	East Pacific Rise	49.0	0.06	−0.42	0.05	23
CH98 DR12	E	East Pacific Rise	44.4	0.25	−0.54	0.03	8
CH98 DR17	T	East Pacific Rise	40.2	0.12	−0.44	0.04	12
CY84 05-08	N	East Pacific Rise	56.1	0.12	−0.38	0.03	8
EN113 02D	N	East Pacific Rise	99.0	0.04	−0.57	0.05	10
EN113 46D	N	East Pacific Rise	111.0	0.05	−0.44	0.07	20
ND15 4	N	East Pacific Rise	51.5	0.07	−0.43	0.04	8
ND21 4	N	East Pacific Rise	46.7	0.07	−0.39	0.05	11
SR2 DR02	N	East Pacific Rise	52.8	0.08	−0.44	0.05	10
SR2 DR03	N	East Pacific Rise	54.9	0.08	−0.33	0.06	8
DS D5	N	Galapagos	167.0	0.07	−0.44	0.06	13
SO40 G136D	T	Gulf of Aden	43.4	0.08	−0.38	0.07	11
SO40 G178D	E	Gulf of Aden	45.1	0.11	−0.38	0.03	21
V3306 39D	N	Gulf of Aden	73.0	0.14	−0.48	0.06	14
V3307 56D	E	Gulf of Aden	86.0	0.21	−0.66	0.09	10
CH31 DR02	E	Mid-Atlantic Ridge	46.6	0.27	−0.45	0.04	22
CH31 DR04	E	Mid-Atlantic Ridge	51.2	0.18	−0.45	0.03	12
CH31 DR11	E	Mid-Atlantic Ridge	45.9	0.24	−0.43	0.03	11
CH31 DR12	T	Mid-Atlantic Ridge	45.7	0.08	−0.46	0.03	23
CL DR01	T	Mid-Atlantic Ridge	61.2	0.16	−0.47	0.05	7
CY82 31 01	T	Mid-Atlantic Ridge	48.3	0.10	−0.47	0.03	7
EN026 14D	E	Mid-Atlantic Ridge	54.0	0.25	−0.66	0.06	10
EN063 23D	N	Mid-Atlantic Ridge	96.4	0.10	−0.29	0.03	13
EW9309 15D	T	Mid-Atlantic Ridge	71.0	0.14	−0.40	0.n	19
ND18 1	E	Mid-Atlantic Ridge	47.4	0.25	−0.36	0.05	11
RC2806 10D	T	Mid-Atlantic Ridge	81.0	0.17	−0.34	0.02	15
TR101 22D	T	Mid-Atlantic Ridge	95.0	0.12	−0.47	0.07	20
TR123 1D	T	Mid-Atlantic Ridge	98.6	0.12	−0.42	0.05	13
TR154 19D	T	Mid-Atlantic Ridge	94.5	0.11	−0.25	0.05	13
KS04 A	E	Red Sea	47.8	0.38	−0.45	0.03	8
KS11 A	E	Red Sea	62.5	0.36	−0.53	0.03	12
KS12	E	Red Sea	68.2	0.24	−0.45	0.03	12
OIBs							
TH28 07		Austral Chain	46.2	0.52	−0.42	0.05	9
TH30 03		Austral Chain	52.4	0.95	−0.35	0.06	11
T4D3#7		Hawaii	82.6	0.27	−0.32	0.02	10
BHVO-2		Hawaii		0.43[d]	−0.49	0.03	46
DTH 03-02		Society Plume	61.3	1.05	0.03	0.07	9
DTH 03-03		Society Plume	55.6	1.11	−0.01	0.03	18
SO47 05DS 1		Society Plume	52.7	1.80	−0.35	0.07	9
SO47 09DS		Society Plume	51.6	1.82	−0.33	0.09	8
SO47 37GC		Society Plume	51.6	2.92	−0.32	0.04	20
TH 09 05		Society Plume	55.7	1.61	−0.49	0.07	8
TH 11 01		Society Plume	47.9	1.65	−0.39	0.03	9
TH 12 01		Society Plume	47.9	1.70	−0.36	0.03	9
TH 14 02		Society Plume	55.5	3.93	−0.57	0.04	9
TH 14 03		Society Plume	50.5	3.36	−0.30	0.03	18
TH 14 05		Society Plume	58.2	3.38	−0.52	0.05	8
TH 21		Society Plume	52.2	2.19	−0.42	0.04	12

[a] Type: N = Normal, $K_2O/TiO_2 < 0.08$; T = Transitional, $0.08 < K_2O/TiO_2 < 0.13$; E = Enriched, $K_2O/TiO_2 > 0.13$; (Marty and Zimmerman, 1999). TiO_2 data from Fisk et al., 1982; Kelley et al., 2013; le Roux et al., 2002; Marty and Zimmermann, 1999; Schilling et al., 1983; Teng et al., 2013.

[b] 95% c.i. = 95% Confidence Interval.

[c] n = number of runs.

[d] K_2O concentration for BHVO-2 from Jochum et al. (2016).

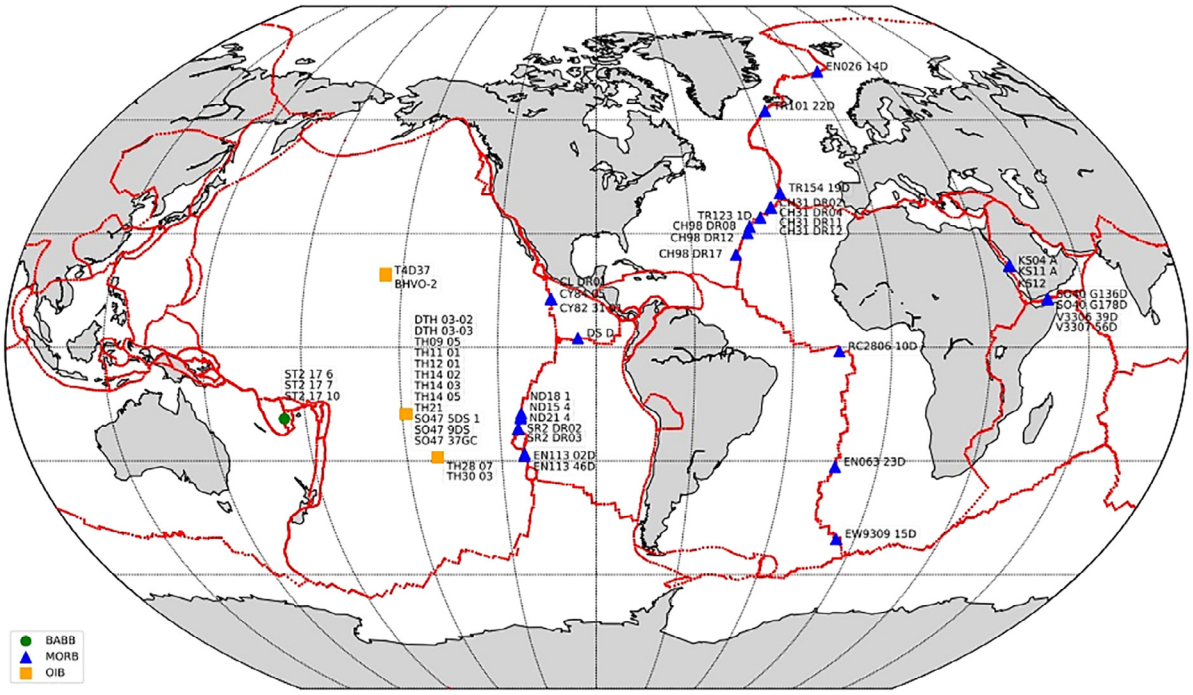

Fig. 1. World map showing the locations of the 51 oceanic basalt samples analyzed in this study.

3. ANALYTICAL METHOD

The analytical method used in this study is similar to the methods reported by other groups (Li et al., 2016; Wang and Jacobsen, 2016a, 2016b; Morgan et al., 2018; Hu et al., 2018). Samples were prepared and analyzed in four steps: digestion in acid, purification for K using ion-exchange chromatography, concentration analysis using iCapQ quadrupole ICP-MS, and finally, isotope analysis using the Neptune Plus MC-ICP-MS.

3.1. Digestion

Pure glass fragments of each sample were selected and ground into a fine powder using an agate mortar and pestle. Both the mortar and pestle were cleaned thoroughly with 4N nitric acid and Milli-Q water before and after each sample. The sample literature K_2O concentrations (see Table 1 footnotes) show that between 40–70 mg of each sample are sufficient for our analyses. Powder was weighed out into Teflon beakers and weights were recorded for each sample (see Table 1).

The samples were then digested in two steps: first, we added 6 mL of a 3: 1 mixture of concentrated hydrofluoric acid (HF) and nitric acid (HNO_3) to each beaker and allowed the beaker to sit under heat lamps for a minimum of five days, at which point the beakers were opened and the solution was allowed to evaporate; second, 3 mL of 6N hydrochloric acid (HCl) was added to each beaker, and beakers were sealed for an additional day before the solution was evaporated for the final time. All samples were completely digested resulting in clear solutions.

3.2. Sample Purification

The sample purification method used here was first proposed by Strelow et al. (1970) and later widely adopted (Humayun and Clayton, 1995; Li et al., 2016; Wang and Jacobsen, 2016a, 2016b; Morgan et al., 2018; Hu et al., 2018). First, dried-down samples from the previous step were rehydrated in 0.7N HNO_3. The samples were then run through one cycle of "big column" followed by one cycle of "small column" ion-exchange chromatography columns. Both columns are filled with AG50-X8 100–200 mesh cation-exchange resin. Several mL (5 for big columns, 2 for small columns) are collected immediately before and after the K cut for the purpose of determining if any K is lost during this process; these are referred to as the pre- and post-cuts.

3.3. Elemental and isotopic analysis

After the K cut was collected from the final cycle of small column chemistry, we analyzed each sample with the Thermo Fisher Scientific iCapQ quadrupole ICP-MS to make sure that K was the primary element collected during the sample purification process and to acquire the concentration of K in each sample. If any other elements are present in abundance >1% relative to K, the sample must be run through another small column cycle to remove these

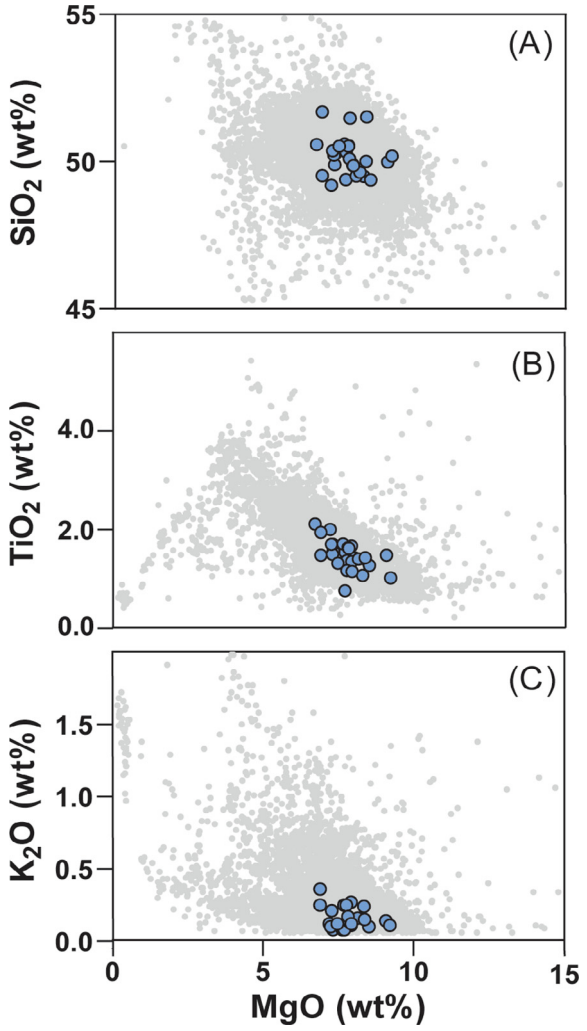

Fig. 2. Geochemical profiles of the MORB samples investigated in this study for which compositional data was available (blue) plotted over the same profiles for the MORB global literature dataset (gray) for (a) SiO_2 vs. MgO, (b) TiO_2 vs. MgO, and (c) K_2O vs MgO. Major element data for samples in this study reported previously (Fisk et al., 1982; Schilling et al., 1983; Marty and Zimmermann, 1999; le Roux and Schilling, 2002; Kelley et al., 2013; Teng et al., 2013). MORB global literature dataset downloaded from PetDB on July 1 2018 (http://www.earthchem.org/petdb) using parameters: "TECTONIC SETTING – Spreading Center; CLASS – Basalt; ALTERATION – Fresh." The secondary bibliography for this dataset can be found in supplementary materials. (For interpretation of the references to colour in this figure legend, the reader is referred to the web version of this article.)

elements, thereby avoiding matrix effects. Additionally, we analyze the pre- and post-cuts collected in both the big and small column cycles to determine if any K was lost outside of our cut; this serves to both double-check our column chromatography methodology, ensuring K recovery of >99%, and make sure the K concentrations are accurate.

The concentrations of each sample acquired by iCapQ were used to match our K bracketing standard (300 ppb NIST SRM3141a) within 3%. Once matched, samples were run through MC-ICP-MS. We measured each sample ~10 times using the sample-standard bracketing technique and the averages of the ~10 measurements are reported. The K isotope compositions are expressed using the per mil (‰) notation of $\delta^{41}K$ for $^{41}K/^{39}K$ ratio, where $\delta^{41}K = [(^{41}K/^{39}K)_{sample}/(^{41}K/^{39}K)_{NIST\ SRM3141a} - 1] \times 1000$. The internal (within-run) reproducibility (95% confidence interval) of ~10 measurements is given for each sample in Table 1, and the typical reproducibility is ~0.05 ‰. The long-term (11 month) external reproducibility, evaluated with geostandard BHVO-2, is ~0.11 ‰ (2S.D.; 2 standard deviation; Chen et al., 2019).

4. RESULTS

The 32 MORB samples had an average of −0.44‰ ± 0.17 (2S.D.), with $\delta^{41}K$ values ranging from −0.25‰ (TR154 19D) to −0.66‰ (EN026 14D) (Fig. 3a). A plot of $\delta^{41}K$ values grouped by MORB type shows no measurable distinction between N-, E-, and T-type MORB (Fig. 4b). The three BABB samples had $\delta^{41}K$ values of −0.40, −0.43, and −0.50‰, giving an average of −0.44‰ ± 0.08 (2S.D.) for the BABB group (Fig. 3b).

The OIB had an average of −0.41‰ ± 0.16 (2S.D.), overall slightly heavier than MORB and BABB; however, this discrepancy is not statistically significant (Fig. 3c). Two samples from the same seamount in the Society Islands (DTH03-02 and DTH03-03) had values ($\delta^{41}K = 0.03$‰ and −0.01‰, respectively) close to seawater (0.10 ± 0.07‰; Wang and Jacobsen, 2016b). A closer examination of these two samples revealed evidence of aqueous alteration in the form of the mineral palagonite, an alteration product from the interaction of seawater. Thus, these samples cannot be classified as "pristine" and were excluded from both our OIB and overall average. Excepting the two outliers above, the OIB group had $\delta^{41}K$ values ranging from −0.30‰ (TH14-03) to −0.57‰ (TH14-02). The slightly greater scattering observed among MORB samples relative to BABB and OIB is likely due to the larger sample size (n = 14 for OIB versus n = 32 for MORB). Results for each group are presented in Fig. 2 and results for each individual sample are presented in Table 1.

5. DISCUSSION

5.1. Variations in K isotopic composition in MORB, BABB, and OIB

The lack of variation between MORB, BABB, and OIB, which all come from different mantle sources (Hofmann, 2007), suggests that there are likely no measurable K isotopic differences between their mantle sources and that the mantle has a homogeneous $\delta^{41}K$ (Fig. 4). Furthermore, plots of $\delta^{41}K$ versus $[K_2O]$, $[SiO_2]$, $[K_2O]/[TiO_2]$, [MgO], and $[Na_{8.0}]$ yielded no observable correlation within any sample group (Fig. 5a–f). $Na_{8.0}$ index (calculated as $[Na_2O] + 0.373 \times [MgO] - 2.98$) reflects the degree of partial melting in the source (higher $Na_{8.0}$ indicates lower degrees of partial melting, and vice versa) and has been used in previous studies to correct for the effects of fraction-

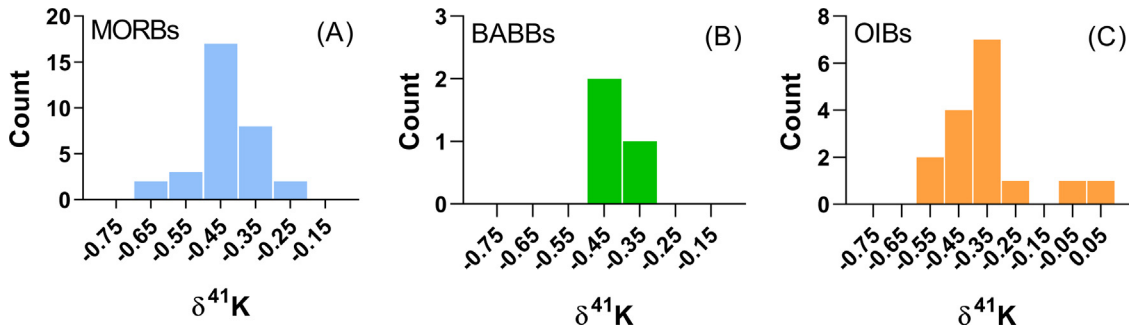

Fig. 3. Distribution of $\delta^{41}K$ values from this study for (a) MORBs, (b) BABBs, and (c) OIBs. The OIB histogram includes two outliers DTH03-02 and DTH03-03 that are excluded from our average calculations and subsequent figures.

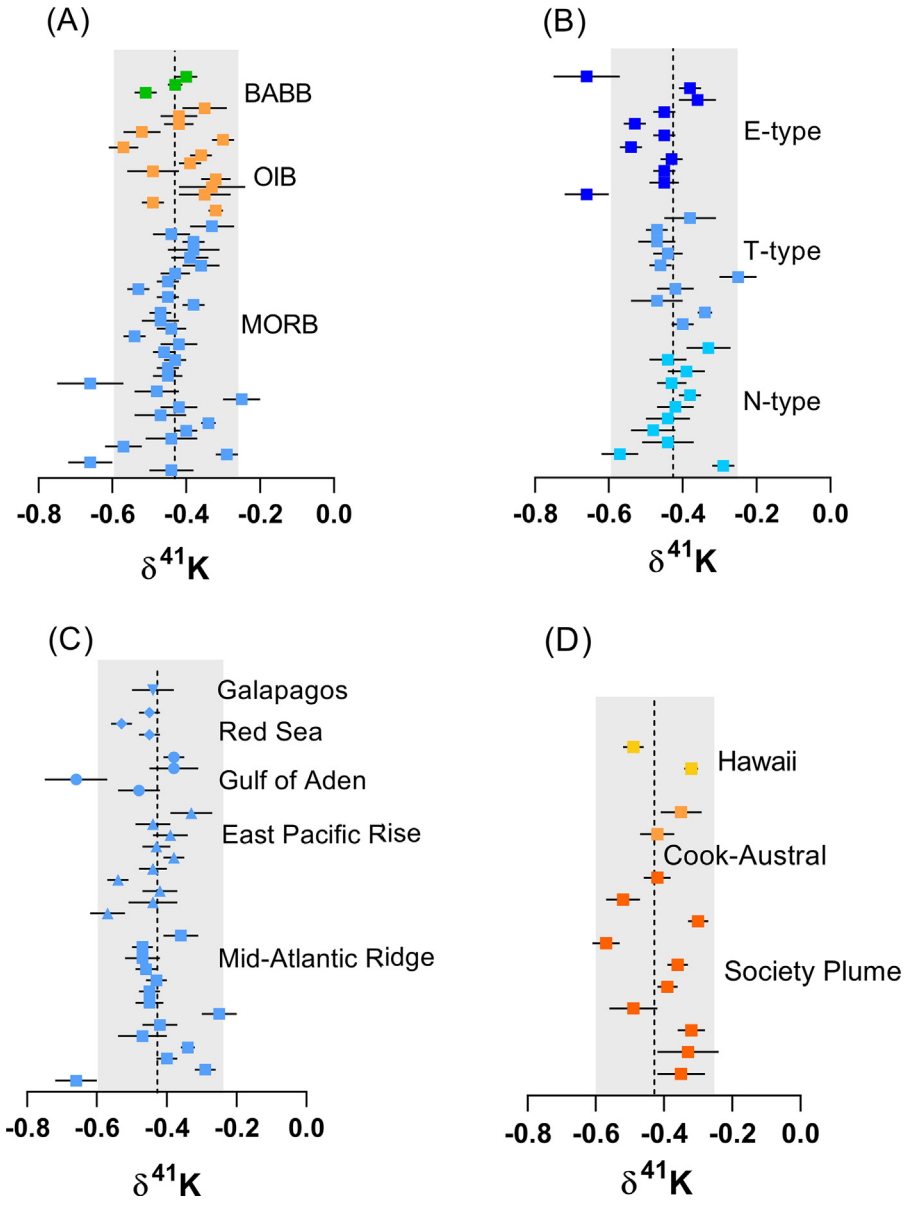

Fig. 4. $\delta^{41}K$ values for pristine samples compared by (a) basalt type, (b) MORB type, (c) MORB source location, and (d) OIB source location. The dashed line and gray shaded area represents the BSE value defined by this study $\pm$ 2 standard deviation.

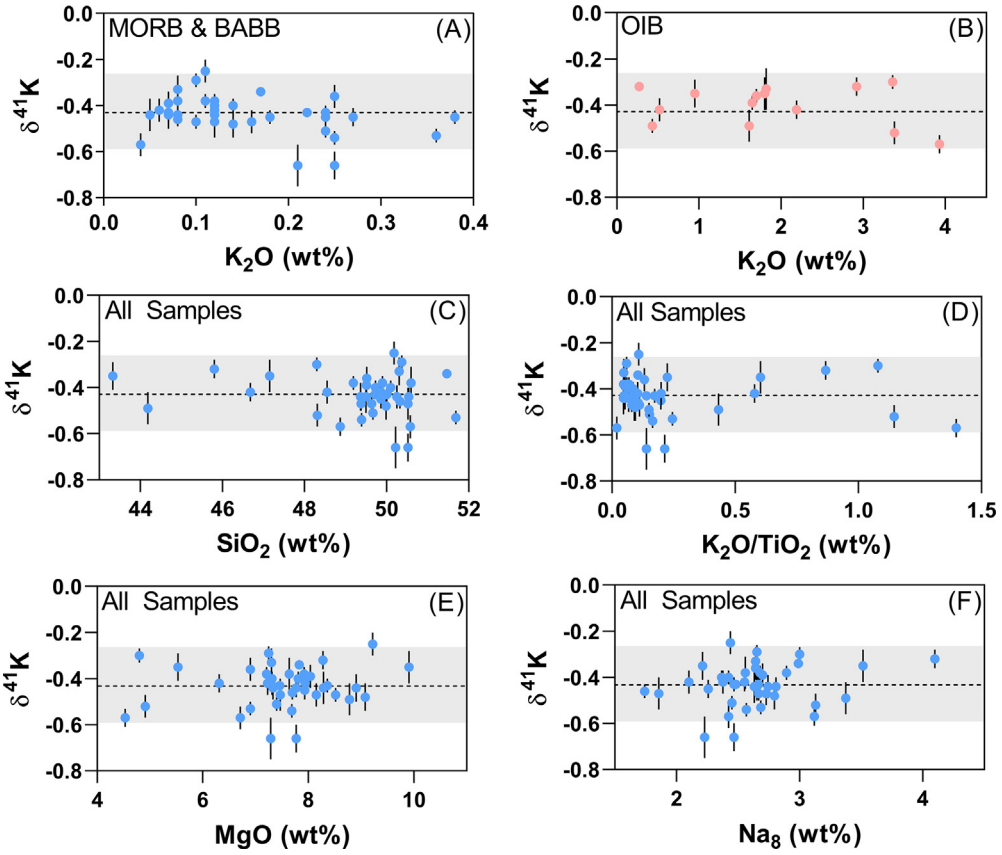

Fig. 5. Plots showing $\delta^{41}K$ values versus (a) K_2O concentration for MORB and BABB samples, (b) K_2O for OIBs, (c) SiO_2 concentration for all samples, (d) K_2O/TiO_2 for all samples, (e) MgO for all samples, and (f) $Na_{8.0}$ value for all samples. $Na_{8.0}$ is used as a measure of degree of partial melting, thus, a trend in plot (d) could be indicative of K fractionation during partial melting. Major element data from Fisk et al. (1982), Kelley et al. (2013), le Roux et al. (2002), Marty and Zimmermann (1999), Schilling et al. (1983), Teng et al. (2013).

ation in the shallow magma chamber (Klein and Langmuir, 1987; Teng et al., 2013). The lack of a resolvable, systematic variation in any of the plots ($\delta^{41}K$ versus $[K_2O]$, $[SiO_2]$, $[K_2O]/[TiO_2]$, [MgO], and $[Na_{8.0}]$) presented in Fig. 5 suggest that all sources have the same original K isotopic composition (i.e., the mantle is homogeneous in terms of K isotope composition) and that this K isotope composition remained unchanged throughout magmatic evolution because K isotopes are not resolvably fractionated by igneous differentiation processes as long as K behaves as a highly incompatible element. This is significant in that it indicates the K isotopic composition of a sample represents the K isotopic composition of its source.

5.2. Estimation of the K isotopic composition of the mantle and implications for interplanetary comparison

Together, MORB ($\delta^{41}K = -0.44 \pm 0.17‰$, 2S.D., n = 32), BABB ($\delta^{41}K = -0.44 \pm 0.08‰$, 2S.D., n = 3), and OIB ($\delta^{41}K = -0.41 \pm 0.16‰$, 2S.D., n = 14) samples from across the world are isotopically homogeneous for K isotopes within uncertainties (Fig. 4a). Our 49 pristine samples had an overall average of $-0.43 \pm 0.17‰$ (2sd). With uncertainty, this average agrees with the BSE value of $-0.48 \pm 0.03‰$ (2S.D.); Wang and Jacobsen, 2016b) defined with three samples. This overall average of global basaltic samples also agrees well with basaltic samples reported from other groups (Li et al., 2016; Morgan et al., 2018; Hu et al., 2018). The average also generally agrees with the K isotopic compositions of nearly all igneous rocks except for pegmatites (Morgan et al., 2018). It also appears, as predicted by theory, that K isotopes do not fractionate during partial melting and other high-temperature igneous differentiation processes in the absence of a significant K-bearing phase (Wang and Jacobsen, 2016a). Thus, from the average of 49 unaltered terrestrial basalts investigated here, we define the K isotopic composition of the mantle as $-0.43 \pm 0.17‰$ (2S.D., n = 49) relative to NIST SRM3141a. Owing to the lack of K isotope fractionation during mantle melting and differentiation of basaltic melts, this mantle average should be representative of the Bulk Silicate Earth (BSE).

This newly defined value for the BSE can be used for interplanetary comparison. As shown in Fig. 6, this K isotope composition of the BSE is marginally higher, however statistically indistinguishable from that of the CI chondrite ($-0.53 \pm 0.10‰$; Wang and Jacobsen, 2016a), the most primitive and most volatile-rich material in the solar system. This conclusion still agrees with Humayun and Clayton (1995), although analytical precision has improved

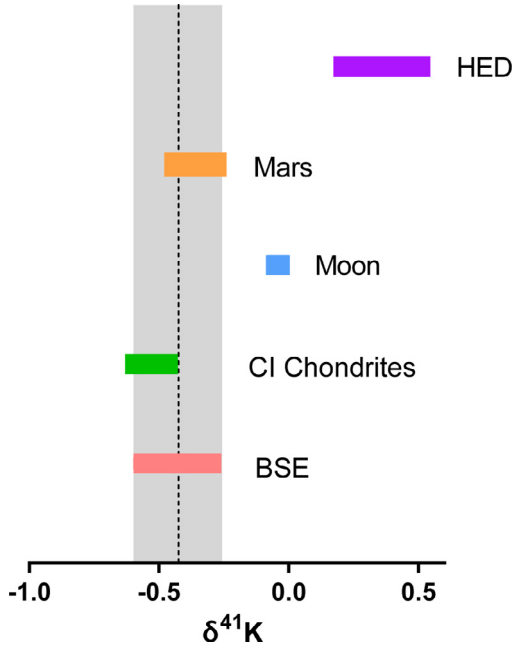

Fig. 6. Comparison showing the average K isotopic compositions ±2S.D. for the Bulk Silicate Earth estimated in this study (also indicated by the dashed line and gray bar), CI Chondrites (Wang and Jacobsen, 2016a), Moon (Wang and Jacobsen, 2016a), Mars (Tian et al., 2018), and Howardite/Eucrite/Diogenite (HED) parent body (Tian et al., 2018).

significantly since then. However, compared to the CI chondrite, the K/U ratio of the Bulk Silicate Earth (12,340 ± 840; Gale et al., 2013) is five times lower than that in CI chondrites (67,160; Lodders et al., 2009). The K/U ratio is an index of volatile depletion because K is a volatile element while U is refractory. Such a depletion of moderately volatile elements (e.g., K) relative to CI chondrites is a characteristic feature of the Earth and all other planetary bodies in the inner solar system (Palme and O'Neill, 2007). It is puzzling that K depletion is decoupled with K isotopic fractionation since Rayleigh-style free vaporization during K loss would generate large isotopic fractionation that could be easily detected with current analytical precision (Humayun and Cassen, 2000). To address this decoupling of K concentration and K isotopic composition, Humayun and Clayton (1995) proposed that incomplete condensation from the solar nebula instead of (kinetic) vaporization of the magma ocean is the reason Earth is depleted in K concentration while the K isotopic composition of the Earth is still indistinguishable from that of chondrites. Alternatively, Hin et al., (2017) suggested the Earth lost all its K during the vaporization generated by accretional collisions and that the current K budget of the Earth was acquired via a late accretion of 20% chondritic materials. Their model can also explain why the K isotopic composition of the Earth is still indistinguishable from that of chondrites while the K abundance of the Earth is only 20% that of chondrites.

This newly defined K isotopic composition of the BSE is also indistinguishable from the K isotopic composition of Martian meteorites (-0.36 ± 0.12 ‰; Tian et al., 2018). However, this K isotopic composition of the BSE is significantly different from that of the Moon (-0.04 ± 0.04‰; Wang and Jacobsen, 2016a). Apollo lunar samples show a significant enrichment of heavy K isotopes compared to terrestrial samples and this result has been explained as the result of a high-energy and high-angular-momentum Giant Impact origin of the Moon from evaporated terrestrial material (Lock et al., 2018); however, this conclusion is still controversial (Dauphas, 2018). Further investigation of whether K isotopes can be used to test different lunar formation models is still needed.

5.3. Potential of K isotopes as a tracer of subducted oceanic crust

The homogeneity of K isotopes among terrestrial basalts, and the suggested lack of significant K isotope fractionation during igneous differentiation and partial melting, is consistent with other isotope systematics in basalts, perhaps most notably that of lithium (Li). Although Li is more compatible than K, the isotope systematics of the two systems are quite similar in oceanic basalts: the Li isotopes in MORB show a relatively restricted range (Chan et al., 1992; Niu et al., 1999; Regelous et al., 1999; Chan et al., 2002; Tomascak et al., 2008; Marschall et al., 2017) and most OIBs are similar to MORBs in terms of Li isotope ratios, except for some HIMU basalts (Nishio et al., 2004; Chan et al., 2009; Vlastélic et al., 2009). These differences were explained as results of either alteration by seawater, assimilation of altered basalts, or diffusion (Chan and Frey, 2003; Chan et al., 2009; Genske et al., 2014).

Altered basalts in both this study and studies of Li isotopes show clear seawater signatures (e.g., Chan et al., 2002, 1992). Both the K and Li isotopic compositions of seawater are significantly different from those of the Bulk Silicate Earth value (i.e., fresh MORB value), proposed reasons for which include high-temperature hydrothermal input, continental weathering, "reverse weathering" characterized by the preferential uptake of ^{39}K and ^{6}Li during the formation of aluminosilicates, and low-temperature alteration of oceanic crust (Bloch and Bischoff, 1979; Staudigel and Hart, 1983; Kronberg, 1985; Santiago Ramos et al., 2018). As shown in the two palagonite-bearing altered basalt samples (DTH03-02 and DTH03-03), their $\delta^{41}K$ values are significantly heavier than those of pristine basalts and are indistinguishable from the seawater value. Thus, through the exchange of K (and Li) between seawater and basalts, the $\delta^{41}K$ (and $\delta^{7}Li$) values of the altered basalts are elevated to values closer to those of seawater. Such low-temperature alteration processes are the major mechanisms responsible for changing the K (and Li) isotope compositions of submarine basalts. Compared to low-temperature seafloor alteration processes, igneous fractionation processes produce negligible K isotopic fractionation. Thus, K isotopes, together with Li isotopes, could be indicators of subducted (altered) oceanic crust. Further study of the K isotope composition of altered samples will be needed to probe the robustness of K as a potential tracer.

6. CONCLUSION

In this study, we measured the K isotopic composition of a wide range of MORB, BABB, and OIB from different localities. The main conclusions to be drawn from this study are:

(1) The mantle is isotopically homogenous for K, within uncertainties, and there is no statistically significant difference in $\delta^{41}K$ values between MORBs, BABBs, and OIBs.
(2) Together, 32 globally sourced MORBs, 3 BABBs, and 14 OIBs define a BSE $\delta^{41}K$ value of -0.43 ± 0.17 (2S.D.).
(3) Post-eruptive processes such as aqueous alteration can significantly fractionate K, and further studies of altered basalts are necessary to determine to what extent K is fractionated by such processes.
(4) The K isotopic composition of pristine, unaltered basalts can likely be used to infer the K isotopic composition of their source, since K does not appear to significantly fractionate during basaltic differentiation.

Declaration of Competing Interest

None.

ACKNOWLEDGEMENTS

The authors thank Dr. Rita Parai at Washington University for her insight on mantle geochemistry, Margaret Duñgo Gritten for assistance with editing and proofreading, and Dr. Wenlei Chen for his assistance in plotting our sample location map. We also thank associate editor Dr. Andreas Stracke and two anonymous reviewers for their thorough reviews and constructive comments.

APPENDIX A

Detailed descriptions of OIB sample sources

Generally, isotopic heterogeneity in the mantle can be accounted for by the mixing and partial mixing of at least five mantle end members: HIMU (high 'μ', or high $^{238}U/^{204}Pb$), EM-1 and EM-2 (enriched mantle 1 and 2, respectively), DMM (depleted MORB mantle), and the hypothesized FOZO (FOcal ZOne, with Pb and Sr values in between HIMU and traditional MORB values) (Zindler and Hart, 1986; Hart et al., 1992; Stracke et al., 2005; Jackson and Dasgupta, 2008).

The 16 OIB samples investigated in this study are mainly pristine basaltic glasses and together reflect contributions from four proposed endmembers: 2 samples are from Hawaii (DMM and FOZO) and 14 samples are from the Polynesian islands (HIMU and EM-2). Hawaii samples investigated here comprise one geostandard (BHVO-2) and one glass. The BHVO-2 geostandard was prepared and distributed by the USGS (United States Geological Survey) and was originally sourced from tholeiitic pahoehoe lava that overflowed from the Halemaumau crater on Kilauea. The other Hawaiian sample investigated here (T4D3 #7) is from the Loihi seamount. Loihi lavas are thought to be a mix of components KOO and KEA with hypothesized mantle endmember FOZO (Bennett et al., 1996; Dixon and Clague, 2001). Together, these two samples reflect contributions from the major end-members found in Hawaiian basalts (e.g., Jackson et al., 2012).

The Polynesian Islands are composed of five main island chains located in the South Pacific: Society, Cook-Austral, Marquesas, Tuamotu, and Pitcairn-Gambier. Investigations of the Polynesia region have indicated that a large-scale upwelling of deep mantle material, or "superplume", may occur beneath this area (Coffin and Eldholm, 1994; Fukao, 1992, 1994; Larson, 1991; Mcnutt and Fischer, 2013; McNutt and Judge, 1990). Polynesian lavas in general are known to be derived from the HIMU, EM-1, and EM-2 mantle endmembers (Teng et al., 2013). Polynesian samples investigated in this study are from the Society ($n = 12$) and Cook-Austral ($n = 2$) chains. Of the Society samples, 1 is from the Rocard Seamount, 8 from the Teahitia Seamount, and 2 from an unnamed seamount termed "Seamount #2" (Marty and Dauphas, 2003). Compared to other oceanic island basalts, Society basalts have intermediate $^{206}Pb/^{204}Pb$ ratios and Sr and Nd isotope ratios ranging from intermediate to extremely high and extremely low, respectively, are enriched in incompatible elements relative to the DMM (e.g., White and Duncan, 2013), and trend towards the EM-2 component on the mantle array.

Both Cook-Austral samples investigated here are from the MacDonald Seamount, an active submarine volcano located at the southeastern terminus of the Cook-Austral chain. The Cook-Austral chain is one of the two regions on Earth (the other being St. Helena in the Atlantic) where the most typical HIMU basalts occur (Kogiso et al., 1997).

APPENDIX B. SUPPLEMENTARY MATERIAL

Supplementary data to this article can be found online at https://doi.org/10.1016/j.gca.2019.06.001.

REFERENCES

Bloch S. and Bischoff J. L. (1979) The effect of low-temperature alteration of basalt on the oceanic budget of potassium. *Geology* **7**, 193.

Chan L.-H., Alt J. C. and Teagle D. A. (2002) Lithium and lithium isotope profiles through the upper oceanic crust: a study of seawater–basalt exchange at ODP Sites 504B and 896A. *Earth Planet. Sci. Lett.* **201**, 187–201.

Chan L.-H. and Frey F. A. (2003) Lithium isotope geochemistry of the Hawaiian plume: results from the Hawaii Scientific Drilling Project and Koolau Volcano. *Geochem. Geophys. Geosyst.* **4**.

Chan L.-H., Lassiter J. C., Hauri E. H., Hart S. R. and Blusztajn J. (2009) Lithium isotope systematics of lavas from the Cook-Austral Islands: constraints on the origin of HIMU mantle. *Earth Planet. Sci. Lett.* **277**, 433–442.

Chan L. H., Edmond J. M., Thompson G. and Gillis K. (1992) Lithium isotopic composition of submarine basalts: implications for the lithium cycle in the oceans. *Earth Planet. Sci. Lett.* **108**, 151–160.

Chen H., Tian Z., Tuller-Ross B., Korotev R. L. and Wang K. (2019) High-precision potassium isotopic analysis by MC-ICP-MS: an inter-laboratory comparison and refined K atomic weight. *J. Anal. At. Spectrom.*.

Dauphas N. (2018) The Origin of the Moon Seen Through an Isotopic Lense. Goldschmidt Conf. Abstr., 523.

Fisk M. R., Bence A. E. and Schilling J.-G. (1982) Major element chemistry of Galapagos Rift Zone magmas and their phenocrysts. *Earth Planet. Sci. Lett.* **61**, 171–189.

Gale A., Dalton C. A., Langmuir C. H., Su Y. and Schilling J.-G. (2013) The mean composition of ocean ridge basalts. *Geochem. Geophys. Geosyst.* **14**, 489–518.

Garnero E. J., Lay T. and McNamara A. (2007) Implications of lower-mantle structural heterogeneity for the existence and nature of whole-mantle plumes. In Special Paper 430: Plates, Plumes and Planetary Processes Geological Society of America. pp. 79–101.

Genske F. S., Turner S. P., Beier C., Chu M.-F., Tonarini S., Pearson N. J. and Haase K. M. (2014) Lithium and boron isotope systematics in lavas from the Azores islands reveal crustal assimilation. *Chem. Geol.* **373**, 27–36.

Hart S. R., Hauri E. H., Oschmann L. A. and Whitehead J. A. (1992) Mantle plumes and entrainment: isotopic evidence. *Science* **256**, 517–520.

Hin R. C., Coath C. D., Carter P. J., Nimmo F., Lai Y.-J., Pogge von Strandmann P. A. E., Willbold M., Leinhardt Z. M., Walter M. J. and Elliott T. (2017) Magnesium isotope evidence that accretional vapour loss shapes planetary compositions. *Nature* **549**, 511–515.

Hofmann A. W. (1997) Mantle geochemistry: the message from oceanic volcanism. *Nature* **385**, 219–229.

Hofmann A. W. (2007) Sampling mantle heterogeneity through oceanic basalts: isotopes and trace elements. *Treatise Geochem. Elsevier*, 1–44.

Hu Y., Chen X., Xu Y.-K. and Teng F.-Z. (2018) High-precision analysis of potassium isotopes by HR-MC-ICPMS. *Chem. Geol.* **493**, 100–108.

Humayun M. and Cassen P. (2000) Processes determining the volatile abundances of the meteorites and terrestrial planets. *Univ. Arizona Press Orig. earth moon*, 3–23.

Humayun M. and Clayton R. N. (1995) Precise determination of the isotopic composition of potassium: application to terrestrial rocks and lunar soils. *Geochim. Cosmochim. Acta* **59**, 2115–2130.

Jackson M. G. and Dasgupta R. (2008) Compositions of HIMU, EM1, and EM2 from global trends between radiogenic isotopes and major elements in ocean island basalts. *Earth Planet. Sci. Lett.* **276**, 175–186.

Jochum K. P., Weis U., Schwager B., Stoll B., Wilson S. A., Haug G. H., Andreae M. O. and Enzweiler J. (2016) Reference values following ISO guidelines for frequently requested rock reference materials. *Geostand. Geoanal. Res.* **40**, 333–350.

Kelley K. A., Kingsley R. and Schilling J.-G. (2013) Composition of plume-influenced mid-ocean ridge lavas and glasses from the Mid-Atlantic Ridge, East Pacific Rise, Galápagos Spreading Center, and Gulf of Aden. *Geochem. Geophys. Geosyst.* **14**, 223–242.

Klein E. M. and Langmuir C. H. (1987) Global correlations of ocean ridge basalt chemistry with axial depth and crustal thickness. *J. Geophys. Res.* **92**, 8089.

Kronberg B. I. (1985) Weathering dynamics and geosphere mixing with reference to the potassium cycle. *Phys. Earth Planet. Inter.* **41**, 125–132.

De Laeter J. R., Böhlke J. K., De Bièvre P., Hidaka H., Peiser H. S., Rosman K. J. R. and Taylor P. D. P. (2003) Atomic weights of the elements: Review 2000 (IUPAC Technical Report).,

Li W., Beard B. L. and Li S. (2016) Precise measurement of stable potassium isotope ratios using a single focusing collision cell multi-collector ICP-MS. *J. Anal. At. Spectrom.* **31**, 1023–1029.

Lock S. J., Stewart S. T., Petaev M. I., Leinhardt Z., Mace M. T., Jacobsen S. B. and Cuk M. (2018) The origin of the moon within a terrestrial synestia. *J. Geophys. Res. Planets* **123**, 910–951.

Lodders K., Palme H. and Gail H.-P. (2009) Abundances of the Elements in the Solar System.

Marschall H. R., Wanless V. D., Shimizu N., Pogge von Strandmann P. A. E., Elliott T. and Monteleone B. D. (2017) The boron and lithium isotopic composition of mid-ocean ridge basalts and the mantle. *Geochim. Cosmochim. Acta* **207**, 102–138.

Marty B. and Zimmermann L. (1999) Volatiles (He, C, N, Ar) in mid-ocean ridge basalts: assesment of shallow-level fractionation and characterization of source composition. *Geochim. Cosmochim. Acta* **63**, 3619–3633.

McDonough W. F. (1990) Constraints on the composition of the continental lithospheric mantle. *Earth Planet. Sci. Lett.* **101**, 1–18.

McDonough W. F. and Sun S.-s. (1995) The composition of the Earth. *Chem. Geol.* **120**, 223–253.

Morgan L. E., Santiago Ramos D. P., Davidheiser-Kroll B., Faithfull J., Lloyd N. S., Ellam R. M. and Higgins J. A. (2018) High-precision41K/39K measurements by MC-ICP-MS indicate terrestrial variability of: δ41K. *J. Anal. At. Spectrom.* **33**, 175–186.

Nishio Y., Nakai S., Yamamoto J., Sumino H., Matsumoto T., Prikhod'ko V. S. and Arai S. (2004) Lithium isotopic systematics of the mantle-derived ultramafic xenoliths: implications for EM1 origin. *Earth Planet. Sci. Lett.* **217**, 245–261.

Niu Y., Collerson K. D., Batiza R., Wendt J. I. and Regelous M. (1999) Origin of enriched-type mid-ocean ridge basalt at ridges far from mantle plumes: the East Pacific Rise at 11°20′N. *J. Geophys. Res. Solid Earth* **104**, 7067–7087.

Palme H. and O'Neill H. S. C. (2007) Cosmochemical estimates of mantle composition. *Treatise Geochem.*, 1–38.

Pearson D. G., Canil D. and Shirey S. B. (2003) Mantle samples included in volcanic rocks: xenoliths and diamonds. *Treatise Geochem. Elsevier.*, 171–275.

Regelous M., Niu Y., Wendt J. I., Batiza R., Greig A. and Collerson K. D. (1999) Variations in the geochemistry of magmatism on the East Pacific Rise at 10°30′N since 800 ka. *Earth Planet. Sci. Lett.* **168**, 45–63.

Le Roux P. and Schilling J. G. (2002) Crystallization processes beneath the southern Mid-Atlantic Ridge (40–55°S), evidence for high-pressure initiation of crystallization. *Contrib. Mineral. Petrol.* **142**, 582–602.

Rudnick R. L. and Gao S. (2003) Composition of the Continental Crust. *Treatise Geochem. Elsevier.*, 1–64.

Santiago Ramos D., Morgan L., Lloyd N. and Higgins J. (2018) Reverse weathering in marine sediments and the geochemical cycle of potassium in seawater: Insights from the K isotopic composition (41 K/ 39 K) of deep-sea pore-fluids.,

Schilling J. G., Zajac M., Evans R., Johnston T., White W., Devine J. D. and Kingsley R. (1983) Petrologic and geochemical variations along the Mid-Atlantic Ridge from 29 degrees N to 73 degrees N. *Am. J. Sci.* **283**, 510–586.

Staudigel H. and Hart S. R. (1983) Alteration of basaltic glass: Mechanisms and significance for the oceanic crust-seawater budget. *Geochim. Cosmochim. Acta* **47**, 337–350.

Stracke A., Hofmann A. W. and Hart S. R. (2005) FOZO, HIMU, and the rest of the mantle zoo. *Geochem. Geophys. Geosyst.* **6**, n/a-n/a.

Strelow E. W. E., Von S., Toerien F. and Weinert C. H. S. W. (1970) Accurate determination of traces of sodium and potas-

sium in rocks by ion exchange followed by atomic absorption spectroscopy. *Anal. Chim. Acta* **50**, 399–405.

Teng F.-Z., Dauphas N., Huang S. and Marty B. (2013) Iron isotopic systematics of oceanic basalts. *Geochim. Cosmochim. Acta* **107**, 12–26.

Teng F.-Z., Dauphas N. and Watkins J. M. (2017) Non-traditional stable isotopes: retrospective and prospective. *Rev. Mineral. Geochem.* **82**, 1–26.

Tian Z., Chen H., Fegley B., Lodders K., Barrat J. A. and Wang K. (2018) Potassium Isotope Differences Among Chondrites, Earth, Moon, Mars, and 4-Vesta — Implication on the Planet Accretion Mechanisms. In 49th Lunar Planet. Sci. Conf. 19-23 March, 2018, held Woodlands, Texas LPI Contrib. No. 2083, id.1276 49.

Tkalčić H., Young M., Muir J. B., Davies D. R. and Mattesini M. (2016) Strong, multi-scale heterogeneity in Earth's lowermost mantle. *Sci. Rep.* **5**, 18416.

Tomascak P. B., Langmuir C. H., le Roux P. J. and Shirey S. B. (2008) Lithium isotopes in global mid-ocean ridge basalts. *Geochim. Cosmochim. Acta* **72**, 1626–1637.

Vlastélic I., Koga K., Chauvel C., Jacques G. and Télouk P. (2009) Survival of lithium isotopic heterogeneities in the mantle supported by HIMU-lavas from Rurutu Island, Austral Chain. *Earth Planet. Sci. Lett.* **286**, 456–466.

Wang K. and Jacobsen S. B. (2016a) An estimate of the Bulk Silicate Earth potassium isotopic composition based on MC-ICPMS measurements of basalts. *Geochim. Cosmochim. Acta* **178**, 223–232.

Wang K. and Jacobsen S. B. (2016b) Potassium isotopic evidence for a high-energy giant impact origin of the Moon. *Nature* **538**, 487–490.

Zindler A. and Hart S. (1986) Chemical geodynamics. *Annu. Rev. Earth Planet. Sci.* **14**, 493–571.

Bennett V. C., Esat T. M. and Norman M. D. (1996) Two mantle-plume components in Hawaiian picrites inferred from correlated Os–Pb isotopes. *Nature* **381**, 221–224.

Coffin M. F. and Eldholm O. (1994) Large igneous provinces: crustal structure, dimensions, and external consequences. *Rev. Geophys.* **32**, 1.

Dixon J. E. and Clague D. A. (2001) Volatiles in basaltic glasses from Loihi seamount, Hawaii: evidence for a relatively dry plume component. *J. Petrol.* **42**, 627–654.

Fukao Y. (1994) Geologic implications of the whole mantle P-wave tomography. *J. Geol. Soc. Jpn.* **100**, 4–23.

Fukao Y. (1992) Seismic Tomogram of the Earth's mantle: geodynamic implications. *Science (80-.)* **258**, 625–630.

Jackson M. G., Weis D. and Huang S. (2012) Major element variations in Hawaiian shield lavas: Source features and perspectives from global ocean island basalt (OIB) systematics. *Geochem. Geophys. Geosyst.* **13**.

Kogiso T., Tatsumi Y., Shimoda G. and Barsczus H. G. (1997) High μ (HIMU) ocean island basalts in southern Polynesia: New evidence for whole mantle scale recycling of subducted oceanic crust. *J. Geophys. Res.* **102**, 8085–8103.

Larson R. L. (1991) Latest pulse of Earth: evidence for a mid-Cretaceous superplume. *Geology* **19**, 547.

Marty B. and Dauphas N. (2003) The nitrogen record of crust-mantle interaction and mantle convection from Archean to Present. *Earth Planet. Sci. Lett.*.

Mcnutt, M. K., Fischer, K. M. (2013). The South Pacific Superswell. In Seamounts, Islands, and Atolls. (1987), Geophys. Monogr. Ser., Vol. 43, (eds. B. H. Keating et Al.), pp. 25–34, AGU, Washington, D. C. pp. 25–34.

McNutt M. K. and Judge A. V. (1990) The superswell and mantle dynamics beneath the South pacific. *Science* **248**, 969–975.

White, W. M., Duncan, R. A. (2013). Geochemistry and Geochronology of the Society Islands: New Evidence for Deep Mantle Recycling. In: Earth Processes: Reading the Isotopic Code. (1996), Geophys. Monogr. Ser., Vol. 95 (eds. A. Basu and S. Hart), pp. 183-206, AGU, Washington, D. C. pp. 183–206.

Associate editor: Andreas Stracke